

High Performance Adaptive Fidelity Algorithms for Multi-Modality Optic Nerve Head Image Fusion

Hua Cao · Nathan Brener · Bahram Khoobehi ·
S. Sitharama Iyengar

Received: 4 May 2010 / Revised: 5 May 2010 / Accepted: 5 May 2010 / Published online: 8 June 2010
© Springer Science+Business Media, LLC 2010

Abstract A high performance adaptive fidelity approach for multi-modality Optic Nerve Head (ONH) image fusion is presented. The new image fusion method, which consists of the Adaptive Fidelity Exploratory Algorithm (AFEA) and the Heuristic Optimization Algorithm (HOA), is reliable and time efficient. It has achieved an optimal fusion result by giving the visualization of fundus image with a maximum angiogram overlay. Control points are detected at the vessel bifurcations using the AFEA. Shape similarity criteria are used to match the control points that represent same salient features of different images. HOA adjusts the initial good-guess of control points at the sub-pixel level in order to maximize the objective function Mutual-Pixel-Count (MPC). In addition, the performance of the AFEA and HOA algorithms was compared to the Centerline Control Point Detection Algorithm, Root Mean Square Error (RMSE) minimization objective function employed by the traditional Iterative Closest Point (ICP) algorithm, Genetic Algorithm, and some other existing image fusion approaches. The evaluation results strengthen the AFEA and HOA algorithms in terms of novelty, automation, accuracy, and efficiency.

Keywords Biomedical imaging · Feature extraction · Heuristic optimization · Image fusion · Image registration

H. Cao (✉) · N. Brener · S. Iyengar
Computer Science Department, Louisiana State University,
Baton Rouge, LA 70802, USA
e-mail: hcao@csc.lsu.edu

B. Khoobehi
Department of Ophthalmology, LSU Eye Center,
New Orleans, LA 70112, USA

1 Introduction

Multi-modality image fusion, which usually requires intensive computational effort, is a very challenging problem because of the possible vast content change and non-uniform distributed intensities of the involved images [1, 2]. In practical clinical applications, automation of image fusion techniques will reduce the number of images reviewed by the physicians and speed up the patient care routine [3]. In the eye clinics, comparison of angiogram grayscale and fundus true color Optic Nerve Head (ONH) images (Fig. 1) is often required in order to identify dynamic aspects of the circulation and evaluate various ONH vascular disorders. By locking the multi-modality ONH images into one single volume, the proposed new algorithms allow ophthalmologists to match the same eye over time and get a sense of disease progression. Ultimately, the new approach allows pinpointing the surgical tools to increase accuracy and overall speed of the surgery.

1.1 Image Fusion Overview

The most widely used methods for image fusion are feature-based and area-based. The feature-based method extracts and matches the common structures (features) from separate images. The feature refers to the salient structures, such as the central line of vessels and the vessel bifurcation points in the ONH network. Mutual Information (MI) [4–6] incorporated with the gradient optimization is a frequently used optimization measurement in area-based non-rigid image registration and fusion. The proposed approach employed the MI concept and simplified it to Mutual-Pixel-Count (MPC). MPC measures the overlapping pixels of the ONH vasculature.

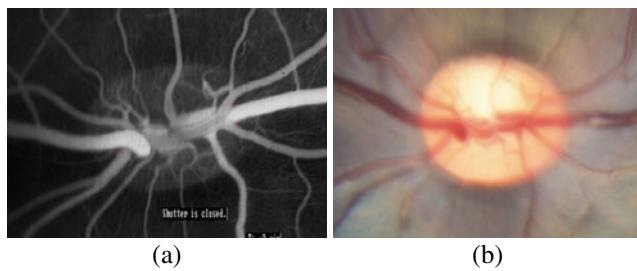


Figure 1 Optic Nerve Head Images. **a** input angiogram grayscale image; **b** reference fundus true color image.

If the images are geometrically aligned, MPC represents the maximal pixel alignment. The feature-based method for feature/control point detection and the area-based method for the optimization fusion are integrated in the proposed approach.

The traditional Iterative Closest Point (ICP) method [7] is often used to reconstruct free-form curves and surfaces from different raw scans. The ICP algorithm firstly gives the initial estimation of the transformation, and then iteratively repeats the transformation estimation by minimizing the RMSE objective function until certain termination criteria are met. The initial estimation and iterative adjustment routine of the new algorithms presented in this paper is an enhancement over the traditional ICP. The comparative estimation will be discussed in Section 4.

The novel ONH image fusion approach made two new contributions to the medical image fusion area. The new contributions are the Adaptive Fidelity Exploratory Algorithm (AFEA) for control point detection and Heuristic Optimization Algorithm (HOA) for adjustment of the control points' initial good-guess. Firstly, the image segmentation extracts ONH vasculature edges using Canny Edge Detector [8]. Secondly, the control points are detected at the vessel bifurcations using the AFEA. Thirdly, shape similarity criteria are used to match the control points that represent same salient features of different images. Finally, HOA iteratively adjusts the initial good-guess of control points at the sub-pixel level in order to maximize the objective function Mutual-Pixel-Count (MPC). The iteration can be terminated either when MPC reaches the maximal or when the maximum allowable loop count is reached.

1.2 Affine Transformation Model

A 2D affine model (Eq. 1) is applied by solving the Gaussian matrix to get $P \in \{a1, a2, a3, a4, b1, b2\}$. Affine model's advantage lies in that it can measure lost information such as skew, translation, rotation, shearing

and scaling that maps finite points to finite points and parallel lines to parallel lines [9].

$$\begin{bmatrix} u_1 \\ v_1 \\ u_2 \\ v_2 \\ u_3 \\ v_3 \end{bmatrix} = \begin{bmatrix} x_1 & y_1 & 1 & 0 & 0 & 0 \\ 0 & 0 & 0 & x_1 & y_1 & 1 \\ x_2 & y_2 & 1 & 0 & 0 & 0 \\ 0 & 0 & 0 & x_2 & y_2 & 1 \\ x_3 & y_3 & 1 & 0 & 0 & 0 \\ 0 & 0 & 0 & x_3 & y_3 & 1 \end{bmatrix} \begin{bmatrix} a_1 \\ a_2 \\ b_1 \\ a_3 \\ a_4 \\ b_2 \end{bmatrix} \quad (1)$$

where (x_1, y_1) , (x_2, y_2) and (x_3, y_3) are the three control points from the input image; (u_1, v_1) , (u_2, v_2) and (u_3, v_3) are the corresponding control points from the reference image.

1.3 Subjects' Image Acquisition

The ONH and overlying vessels were imaged with a Topcon TRC-50EX fundus camera (Fig. 2) attached to a hyperspectral imaging system [10]. The primates were cynomolgus monkeys of 4–4.5 years of age and 2.5–3 kg body weight with normal eyes. The experimental monkey was anesthetized with the intramuscular ketamine (7–10 mg/kg), xylazine (0.6–1 mg/kg), and intravenous pentobarbital (25–30 mg/kg) [11]. ONH images were obtained with inspiration of pure oxygen and room air at the controlled intraocular pressures of 10 mm Hg sustained for up to 10 min after the eyes were dilated.

1.4 Image Binarization and Edge Extraction

In the ONH network, objects of interest are the ONH vessels, i.e. arteries and veins. Firstly, both of the reference and input images are binarized (Fig. 3 (a) and (b)) using a clustering threshold developed by Otsu [12]. Otsu's thresholding, one of the most referenced thresholding methods,

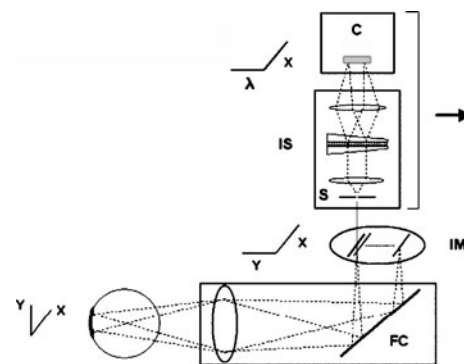


Figure 2 The optical diagram of an ONH hyperspectral imager with a fundus camera. The region of interest is imaged with a fundus camera (FC). The intermediate image (IM) is formed at the slit (S) of an imaging spectrograph (IS). The output spectrum is focused on a CCD camera (C). Dotted lines are the light collection path. The spectrograph and camera are translated following the y axis. Motion is controlled to create a 1:1 ratio between adjacent pixels in the x direction and lines in the y direction [10].

gives satisfactory results when the numbers of pixels in each class are close to each other [13]. The threshold is a normalized intensity value that lies in the range [0, 1]. If the input intensity is less than Otsu’s threshold, the output binary pixel is marked as 0 (black); otherwise, the output pixel is marked as 1 (white).

The Canny operator finds edges by looking for local maxima of the gradient of the input image (Fig. 3 (c) and (d)). Canny’s method detects the edges at the zero-crossings of the second directional derivative of the image. It performs the zero-crossings of

$$\frac{d^2(G \times I)}{dn^2} = \frac{d\left(\left(\frac{dG}{dn}\right) \times I\right)}{dn} \quad (2)$$

It uses two thresholds for detecting strong and weak edges. The zero-crossings are corresponding to the first directional-derivative’s maxima and minima in the direction of the gradient. Each pixel’s edge gradient is computed and compared with the gradients of its neighbors along with the

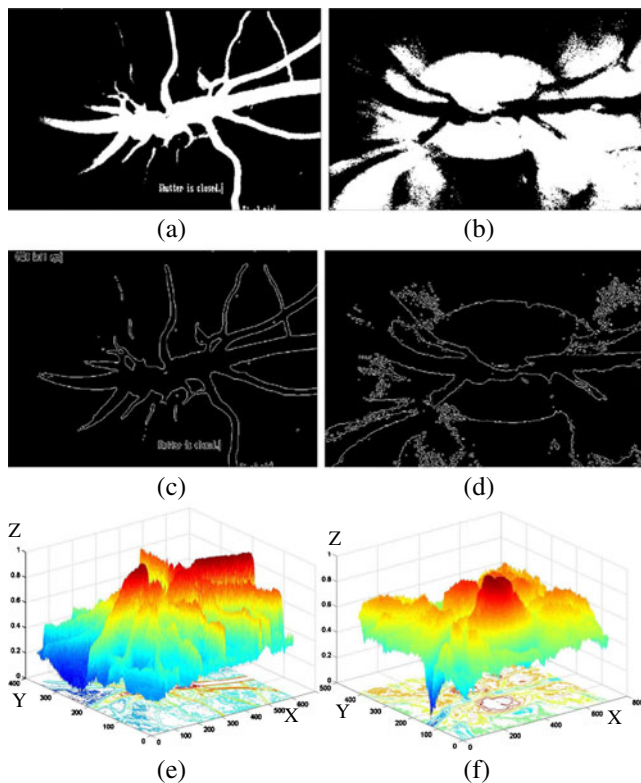


Figure 3 **a** Binarized input image from the grayscale angiogram image; **b** Binarized reference image from the true color fundus image; **c** Canny edges of the reference image; **d** Canny edges of the input image; **e** 3D shaded surface plot of the reference image; **f** 3D shaded surface plot of the input image. The *X*-*Y* axis of the 3D shaded surface plot corresponds to the original image size. The height *Z* axis is a single-valued function defined over a geometrically rectangular grid. *Z* specifies the color data as well as surface height, so that color is proportional to surface height with range of [0, 1]. It can be observed from (e) and (f) that all ONH salient features are preserved in the Canny edges.

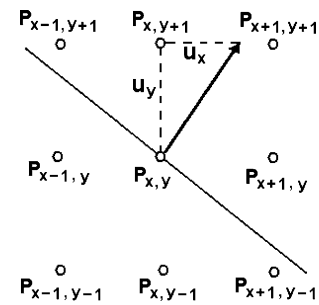


Figure 4 Canny Edge Detection—Localization of Maxima.

gradient direction. The gradient magnitude at $P_{x+1, y+1}$ and $P_{x-1, y-1}$ (Fig. 4) can be calculated as:

$$P_{x+1,y+1} : G(P_{x+1,y+1}) = \frac{u}{u_y} G(x+1, y+1) + \frac{u_y - u_x}{u_y} G(x, y+1) \quad (3)$$

$$P_{x-1,y-1} : G(P_{x-1,y-1}) = \frac{u}{u_y} G(x-1, y-1) + \frac{u_y - u_x}{u_y} G(x, y-1) \quad (4)$$

Canny operator is less likely than the others to be “fooled” by noise, and more likely to detect true weak edges [8].

2 Control Point Detection

2.1 Problem Formulation

In the ONH network, features are the vessel centerline or vasculature bifurcations, also known as the control points. As required by the 2D affine transformation model, three control points are identified at the reference image and three corresponding ones are located at the input image (Eq. 5).

$$(CP_1, CP_2, CP_3) \Leftrightarrow (CP'_1, CP'_2, CP'_3) \quad (5)$$

where, CP_1, CP_2 and CP_3 are the control points from the reference image and each of them represent one feature of the ONH vessels; CP'_1, CP'_2 and CP'_3 are the corresponding control points from the input image and each represent same feature as CP_1, CP_2 , and CP_3 respectively.

Control points detection is an essential step of an image fusion approach. Good control point selection will ensure fused image generated at a short running time. Bad control point selection will significantly increase the computation cost, or even cause the image fusion fail. Some particular vessel abnormalities make images not necessarily matching the ONH structures. Even when structure and function correspond, the abnormality still happens if inconsistency exists between structural and functional changes. Further

more, angiogram grayscale images usually have higher resolution and are rich in information, whereas fundus color images have lower resolution and are indeed abstract with some details or even missing some small vessels. Practically, those situations will create difficulties in extracting the control points because the delineation of vein boundaries may not be precise. The AFEA algorithm presented in this paper is able to conquer these difficulties and give an initial good-guess of the control points.

2.2 Eight-Connectivity Chain Code

In the AFEA algorithm, edge pixels are processed by using an eight-connectivity chain code (Table 1). An edge curve can be represented by an integer sequence based on the position of the current edge pixel N_i to their eight neighbors at the 2D spatial domain:

$$N_i \in \{1, 2, 3, 4, 5, 6, 7, 8\} \tag{6}$$

where, numerical digits 1–8 correspond to different angles.

The ONH vessel edges detected through image segmentation present the chain codes in such rule that:

- 1) If southeast “5” neighbor is detected, neither east “3” neighbor nor south “1” neighbor should be detected;
- 2) If northwest “6” neighbor is detected, neither west “4” neighbor nor north “2” neighbor should be detected;
- 3) If southwest “7” neighbor is detected, neither west “4” neighbor nor south “1” neighbor should be detected;
- 4) If northeast “8” neighbor is detected, neither east “3” neighbor nor north “2” neighbor should be detected.

2.3 Adaptive Fidelity Exploratory Algorithm (AFEA)

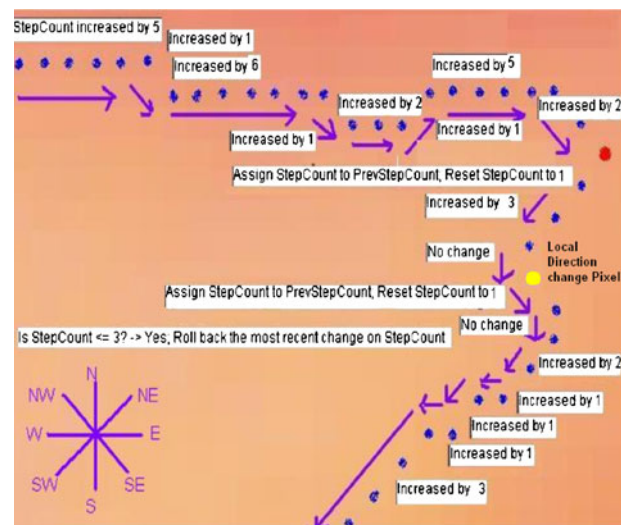
Generally speaking, there are two broad groups of vasculature control point process methods. The first group is called “pixel-processing approach” [14]. It uses matched filtering, segmentations, thinning, and bifurcation identification by processing every pixel and imposing numerous operations at each pixel. The “pixel-processing approach” scales poorly

Table 1 Chain code representation.

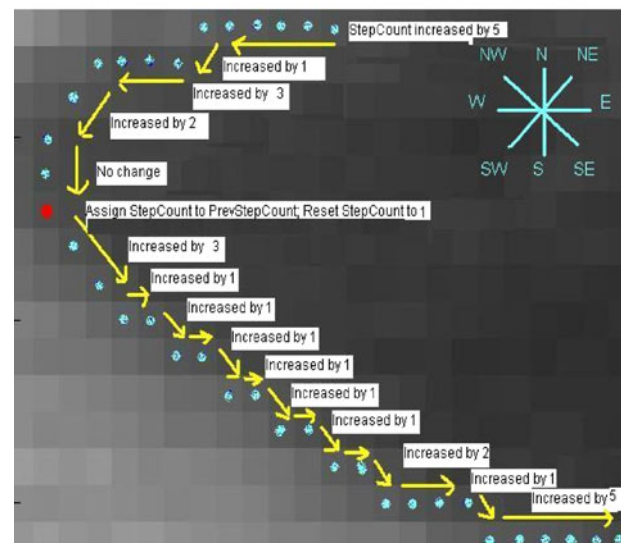
Chain code	Direction	Angle
1	South	270 °
2	North	90 °
3	East	0 °
4	West	180 °
5	Southeast	315 °
6	Northwest	135 °
7	Southwest	225 °
8	Northeast	45 °

with large image size and can hardly meet short computation deadlines. The second group is called “exploratory algorithms” [15, 16]. The AFEA algorithm can be classified into the second group. In the ONH network, the control points are selected at the vessel bifurcations on Canny edges. A vessel tracking is efficiently implemented on Canny edges without traveling at every pixel.

The AFEA traces the image contour by locating an initial point and exploiting the local neighbors. Firstly, the entire image is split into two equal size blocks of West and East. Given the vessel bifurcation feature of ONH network, splitting images into two blocks is able to improve the efficiency of vessel tracking and accuracy of bifurcation locating. Secondly, the edge pixels are processed from west to east and from north to south at the West Block (Fig. 5).



(a) An example for the step count calculation on West Block.



(b) An example for the step count calculation on East Block.

Figure 5 Examples for the step count calculation. Blue pixel—edge; red pixel—control point candidate; yellow pixel—local direction change.

Edge pixels at the East Block are processed in the opposite direction (Fig. 5). The initial points are located at the northwest corner and northeast corner on Canny edges at the West Block and East Block, respectively. The eight-connectivity chain code rule prevents the ambiguity to choose the next to-be-processed pixel, because there is always at most one connected neighbor, if there is any, next to the current pixel. However, if there is no next edge pixel, a scanning will be triggered by following the same direction of the vessel tracking from the current point till it finds an unprocessed edge pixel. When every edge pixel of the entire ONH network has been processed, the tracking will be terminated.

At the West Block, as long as the edge pixels are heading toward East, no matter toward North East, East or South East, the current direction is marked as “East” and the step count is incremented by 1. If the direction starts to change, i.e. change from East to West, the step count needs to be compared to a rollback threshold. If smaller, roll back the most recent change of the step count; otherwise, keep the new step direction. The rollback threshold is used to determine whether or not a direction change is local. When a rollback is triggered, it means the direction change is local, and thus it should not be considered as a real vessel bifurcation. The local direction change pixels (the yellow pixel on Fig. 5 (a)), which usually come from the curved part on the ONH vessel edges, do not represent the real vessel bifurcations. The (X, Y) coordinate of a non-local changing pixel is a possible control point’s coordinate that the algorithm will determine later. If the step count is equal to a maximum allowed step count threshold, and the previous direction’s step count is greater than or equal to the maximum allowed step count threshold, the most recent possible control point is determined as a true control point candidate (Figs. 6–7).

2.4 Outlier Control Point Detection

Rather than only preserving the real vessel bifurcations, the edge detection process could create extra edge bifurcations due to the gray level property of the vessels. These extra edge bifurcations are the outlier control points (Fig. 7 (a)). They are not representing the true bifurcation features of the ONH vasculature. Removing outliers are important because the mis-detected control points could cause mis-matched control point pairs between the reference and input images and furthermore cause fusion failure.

In the AFEA algorithm, outlier control points can be removed by detecting the opposite global direction change pixels. In the West Block, the direction change sign for control point identification is from heading

eastward to westward. If there is any detected direction change pixel having the opposite direction change, i.e. from heading westward to eastward, this direction change pixel is identified as an outlier control point. In the East Block, the direction change pixel will be marked as an outlier if its direction change sign is from heading eastward to westward.

2.5 Control Point Pair Matching

The detected control points need to be matched as one pair per match using a certain matching criterion. The Shape Similarity Criteria [17–19], which are able to identify an unknown shape by matching it to the most similar shape model, are employed to match the control points into three pairs as required by the 2D affine transformation. The shape similarity based matching process takes the following procedure. Firstly, the control points are divided into a certain number of groups. The image having less number of control points is taken as the grouping base. Suppose image I_1 has n control points, and image I_2 has m control points, and $m < n$, then m will be the group number determining that how many groups of control points it will have. Secondly, each control point in I_1 is combined with each control point in I_2 , and there are totally $m \times n$ control point pairs. The distance $|d|$ between each control point pair is then calculated within each group using Eq. 7.

$$|d| = \sqrt{(x_1 - x_2)^2 + (y_1 - y_2)^2} \quad (7)$$

where (x_1, y_1) is the coordinate of one control point; (x_2, y_2) is the coordinate of the other control point. Thirdly, inside each group, the pair with minimum $|d|$ is chosen. The assumption it uses the minimum distance as matching criteria is based on the fact that the two images do not have huge rotation, shearing or translation, and thus the same features on each image are close to each other. If two or more control points in one image match the same control point in the other image, the true match will always has smaller $|d|$ than the false match based on the Shape Similarity Criteria assumption. Finally, the method selects the three smallest distance $|d|$ control point pairs as the final (x, y) and (u, v) for the 2D affine transformation.

3 Heuristic Optimization

3.1 Problem Formulation

An initial good-guess of the control points improves the probability of convergence and the quality of the fused image. The initial guess, which is close to the optimal

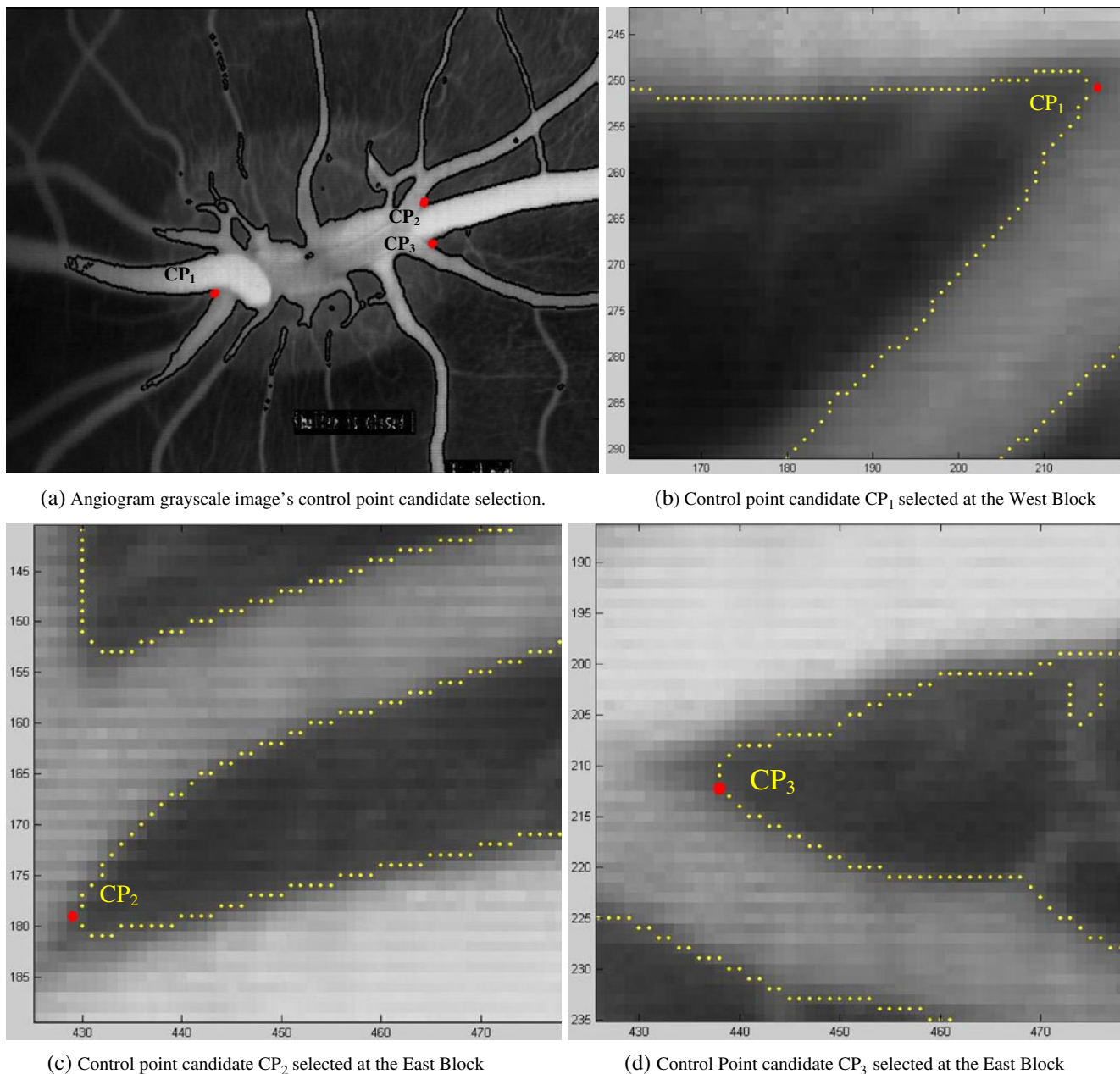


Figure 6 Angiogram grayscale image's control point selection; Black pixel—edge; red pixel—control point candidate.

result, is not an accurate solution because the Canny operator detects edges at the fuzzy ONH vasculature. Figure 8 (a) are the fused image based on the initial guess, where the fundus image does not have a maximum angiogram overlay. Therefore, an optimization procedure is required to adjust the initial good-guess control points in order to achieve the optimal fusion result. Such process can be formulated as a heuristic problem of optimizing an objective function that maximizes the Mutual-Pixel-Count between the reference and input images. The algorithm finds the optimal solution by continuously refining the transformation parameters in an ordered way. During the

iteration, the reference image's control points' (u, v) coordinates are fixed. Only input image's control points' (x, y) coordinates are subject to adjustment. The fused image is assumed to be optimal when the objective function is maximized.

3.2 Objective Function: Mutual-Pixel-Count (MPC)

Mutual-Pixel-Count measures the ONH vasculature overlapping for corresponding pixels in both images. When the vasculature pixel's transformed (u, v) coordinates on the input image correspond to the vasculature pixel's coordi-

nates on the reference image, MPC is incremented by 1. MPC is assumed be maximized when the image pair is perfectly geometrically aligned by the transformation. The problem can be mathematically formulated as maximization of the following objective function:

$$f_{mpc}(x, y, u, v) = \sum_{\substack{u, v \in ROI \\ I_{ref}(x, y) = 0 \text{ and } I_{input}(u, v) = 0}} I_{input}(T_x(u, v), T_y(u, v)) \quad (8)$$

where,

$$T_x = a_1u + a_2v + b_1 \quad (9)$$

$$T_y = a_3u + a_4v + b_2 \quad (10)$$

The objective function f_{MPC} denotes the Mutual-Pixel-Count. T_x (Eq. 9) and T_y (Eq. 10) are the transformations for u and v coordinates of the input image. The Region-of-Interest (ROI) is the ONH vasculature region where MPC is calculated on. Parameters $\{a1, a2, a3, a4, b1, b2\}$ is obtained using Eq. 1.

After the image segmentation, the binary images of the input and the reference images are obtained, i.e. I_{input} and I_{ref} (Fig. 3 (a) and (b)). Only black pixels from both images contribute to MPC. The ideal case is that all zero (black) pixels of the input image are mapped onto zero pixels of the reference image. This calculation can be formulated in pseudo codes as follows:

```
if B(x, y) = B(xu, yv)
    then MPC = MPC + 1;
end if
```

where B is a binary 2D map. In this binary map, 0 denotes the vessel pixel (black) and 1 denotes the background pixel (white). For the affine transformation T and all pixels (u_i, v_i) , where

$$(u_i, v_i) \in ROI, (x_u, y_v) = T(u, v) \quad (11)$$

3.3 Heuristic Optimization Algorithm (HOA)

To solve the optimization problem, a global optimization scheme (e.g. the brute force exhaustive search technique) can guarantee the successful outcome of the global maxima but with the tradeoff on excess computation cost. In the real scenario, the search domain range has to be narrowed down in order to accelerate the execution. A local optimization scheme is usually applied to reduce the computation cost. However, local optimization can be attracted to local maxima [20].

The HOA algorithm does not guarantee that the objective function always reaches the global maxima. The reason is not because the heuristic method is inefficient, but

the fact that the features and objects on the reference and input images are not identical in most cases.

In HOA, the initial movement direction is randomly determined. Suppose ∇M is the changed volume of f_{MPC} . MPC_{prev} is the previous f_{MPC} prior to the movement, and MPC is the current f_{MPC} after the movement, then:

$$\nabla M = MPC - MPC_{prev} \begin{cases} > 0 : \text{Keep moving the coordinate} \\ & \text{toward the same direction.} \\ \leq 0 : \text{Step(1) - Stop } u \text{ or } v \text{ movement in} \\ & \text{that same direction;} \\ & \text{Step(2) - Move the coordinate} \\ & \text{toward a new random direction} \end{cases} \quad (12)$$

This process can be formulated in pseudo codes as follows:

```
Assign startPixel(u, v) to currentPixel;
Initialize nextMPC to 0;
For all four neighbors of currentPixel
    Locate a neighbor (ui, vi) of currentPixel in an ordered way;
    // i is the number of visited neighbors
    if (fMPC(ui, vi) > nextMPC)
        Assign fMPC(ui, vi) to nextMPC;
        Assign (ui, vi) to currentPixel;
    else
        break;
    end if
end for loop
```

Coordinates' adjustment is iteratively implemented until one of the following convergence criteria is reached:

1. Predefined maximum number of loops is reached.
2. The updated MPC is smaller than ϵ , i.e.

$$|f_{MPC}^{n+1}(x, y, u, v) - f_{MPC}^n(x, y, u, v)| \leq \epsilon \quad (13)$$

where,

ϵ is a very small non-negative threshold; $f_{MPC}^{n+1}(x, y, u, v)$ is the updated MPC; and $f_{MPC}^n(x, y, u, v)$ is the current MPC.

3.4 Implementation

The experimental monkey was anesthetized repeatedly every 30 min as required to maintain the animal in deep, stage IV anesthesia. However, the anesthetics procedure cannot be simply repeated on humans only for the eye examination purpose. The clinical goal of the ONH image fusion (Figs. 8 and 9) is to achieve a maximum angiogram overlay on the fundus image. In all cases, fused images are generated following binarization, edge extraction, control point detection using the AFEA algorithm, and optimization using the HOA algorithm.

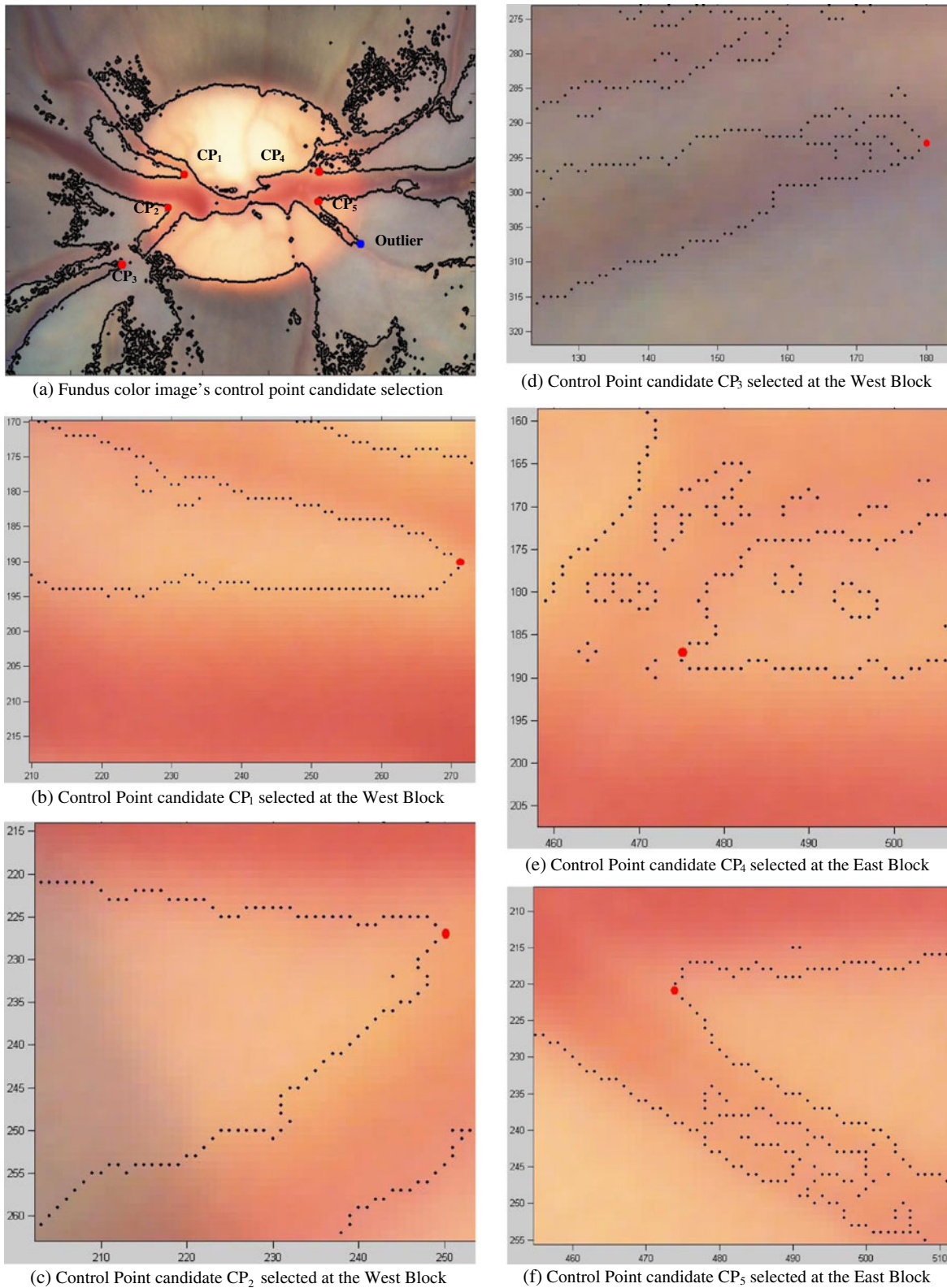


Figure 7 Fundus color image's control point selection. Black pixels are edges; red pixels are control point candidates; the blue pixel on (a) is the outlier.

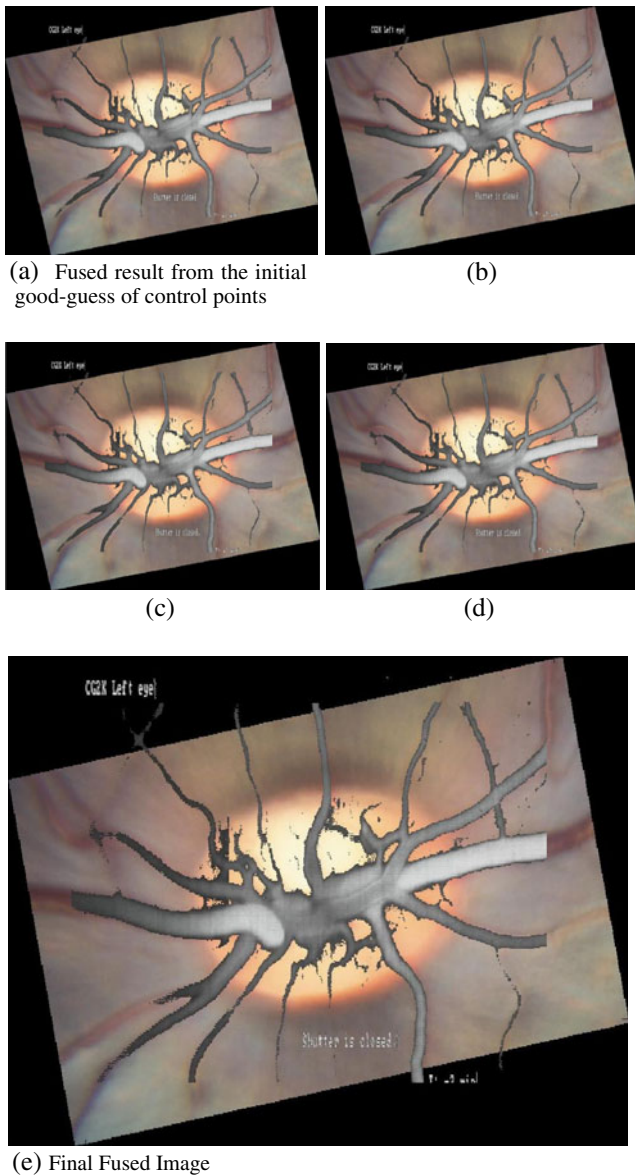


Figure 8 Fused image improvement during the iteration. f_{MPC} (a)–(e) = 30372, 30888, 30914, 31134, 32277.

4 Qualitative Evaluation

The performance of the proposed AEFA and HOA algorithms were compared to the results of Centerline Control Point Detection Algorithm, Root Mean Square Error (RMSE) minimization objective function employed by the traditional Iterative Closest Point (ICP) algorithm, and Genetic Algorithm. In addition, some other existing image fusion approaches were discussed in terms of running time. The time series, objective function f_{MPC} , and the visual fusion results have been extensively used in this evaluation to measure and compare the performance of different fusion methods. The evaluation results strengthen

the AFEA and HOA algorithms in terms of novelty, automation, accuracy, and efficiency.

4.1 Genetic Optimization Algorithm

Genetic Algorithm (GA) is a well-known global optimization technique which has been employed to solve numerous optimization problems, including biology, chemistry, medical physics, and medical image processing [21, 22]. Crossover and mutation are the two frequently used GA operations. In this comparative GA analysis, there are totally 3 groups of data populations, and each group stands for one control point from the input image. The population size remains same for each generation. Each individual is an unsigned char array. Each element in the array is a random number S_n .

$$S_n \in \{0, 1, 2, 3\} \tag{14}$$

where, 0, 1, 2, and 3 stand for the possible moving direction toward East, West, North and South, respectively. The initial 3 individuals are the coordinates of the initial guess of the control points $((x_1, y_1), (x_2, y_2), (x_3, y_3))$. Each individual's fitness is estimated by the same objective function f_{MPC} . Half of the total individuals (parents+children) with higher f_{MPC} are selected. The offspring generation is iteratively produced till the termination condition is reached. 40 simulations with the final GA-based fused images were carried out. The average rate of running time and the objective function f_{MPC} showed that the HOA achieved a better optimization with a higher f_{MPC} than GA and lower running time consumption (Table 2) (Fig. 10).

4.2 Centerline Control Point Detection Algorithm

For evaluating and comparing the proposed AFEA algorithm to the Centerline Control Point Detection Algorithm

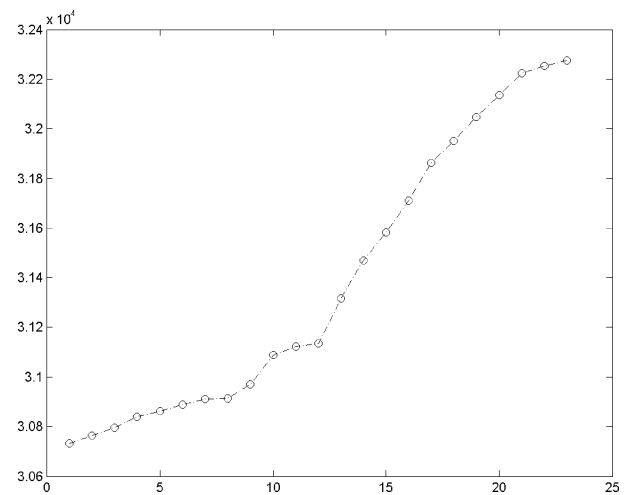


Figure 9 f_{MPC} increasing during optimization (Y-axis is the f_{MPC} ; X-axis is the loop count).

Table 2 Comparison of GA and HOA's average performance.

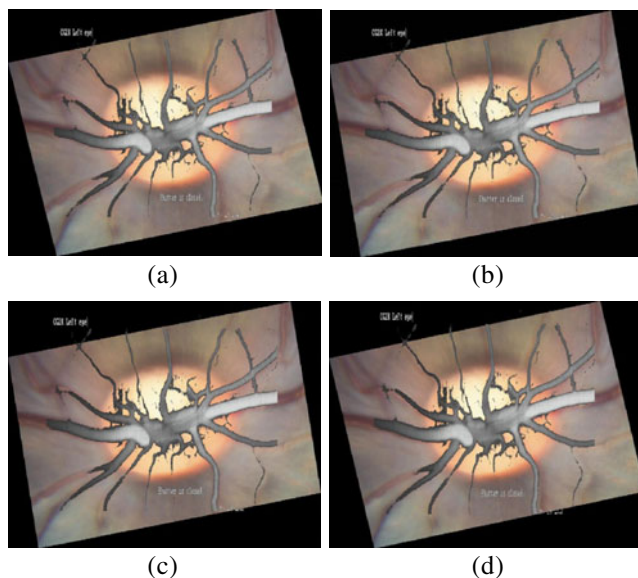
Algorithm	f_{MPC}	Running time
GA	31830	7.3 minutes
HOA	32277	1 minute

reported by Laliberte in literature [23], the same ONH image pairs were fused by applying both of the HOA algorithm and the Genetic Algorithm. In Laliberte's algorithm, the vessel thin image is firstly created using a thinning algorithm that guarantees a one-pixel width. Secondly, pixels with three or four neighbors were identified as the control points. Thirdly, control points were matched by utilizing the following criteria:

- 1) Control point pair located inside a distance threshold;
- 2) With same number of neighbors;
- 3) Distance between angle is less than a threshold σ ;
- 4) Eliminate the one without matches.

The initial control point's objective function f_{MPC} is 7134. They are lower than the proposed AFEA algorithm's result of 30372. The final f_{MPC} after applying the HOA is 29720, which is apparently lower than the final f_{MPC} by applying the AFEA algorithm, i.e. 32277 (Table 3). Therefore, the AFEA algorithm has provided a better performance than the Centerline Control Point Detection Algorithm in terms of f_{MPC} (Fig. 11).

Furthermore, Laliberte's centerline control point detection algorithm has 10 threshold parameters of which 7 are dependent on the image resolution and 3 left main free. More threshold parameters the algorithm has, more

**Figure 10** Fused image generated by GA: **a** $f_{MPC}=31227$; **b** $f_{MPC}=32007$; **c** $f_{MPC}=32185$; **d** $f_{MPC}=32220$.**Table 3** Comparison of centerline control point detection algorithm with the AFEA algorithm.

Objective function f_{MPC}	Centerline algorithm	AFEA algorithm
Initial f_{MPC}	7143	30372
GA final f_{MPC} (Average)	29337	31861
HOA final f_{MPC}	29720	32277

human's intervention is required when parameters need adjustment, and hence less automation level the program is. In the AFEA and HOA algorithms, there are totally 9 adjustable threshold parameters (Table 4). Among them, 5 are dependent on the image resolution/size and 4 are left main free.

4.3 RMSE Minimization—ICP's Objective Function

Root Mean Square Error (RMSE) between the coordinates of the reference image and the transformed image has been used by the Iterative Closest Point algorithm as the objective function. RMSE is defined as:

$$\text{RMSE} = \sqrt{\left(\sum_{i=0}^N (x_{true} - x_{reverse})^2 + (y_{true} - y_{reverse})^2 \right) / N} \quad (15)$$

where N is the number of common pixels existing in both images. The x_{true} and y_{true} are the true coordinates from the reference image. The $x_{reverse}$ and $y_{reverse}$ are the reverse transformed coordinates by applying the reverse transformation of the known 2D affine polynomials. Figure 12 displays 6 selected intermediate fused images during RMSE minimization. It can be observed that the fused image's quality is not necessarily getting improved when RMSE is becoming smaller. There is no clear relationship between the quality of the fused image and the value of RMSE that can follow a certain pattern. Therefore, RMSE is not an ideal objective function when applying to multi-modality ONH image fusion.

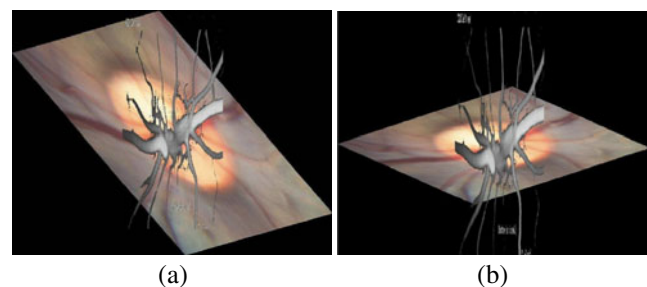
**Figure 11** Fused image by applying the Centerline algorithm. **a**: by HOA with $f_{MPC}=29720$; **b**: by GA algorithm with $f_{MPC}=29337$.

Table 4 Threshold parameters of AFEA and HOA algorithms.

Parameters	Annotation
(1) Comparing Edge	ROI's <i>X</i> -axis for estimating f_{MPC}
(2) Otsu's threshold	Image binarization [12]
(3) Adjusted Otsu's Threshold	Image binarization
(4) Vasculature Extraction Threshold	Making either reference or input image transparent, so that one can be overlaid on the other
(5) Black Area Percentage	Determining whether parameter (2) or (3) should be used
(6) Max Steps on Gray Image	A maximum allowed step count threshold on the grayscale image for the control point identification
(7) Max Steps on Color Image	A maximum allowed step count threshold on the color image for the control point identification
(8) Roll Back Threshold	Determining whether or not a direction change pixel is a final control point candidate
(9) Maximum loop count	Determining when the HOA stops

4.4 Other Existing Data Fusion Approaches

In the manual fusion approach, the ophthalmologist identifies control points at vessel bifurcations, which are common to both images that are to be registered. The control points placed by the experts seemed appropriate. However, the fusion result might not be optimal at many cases. The disadvantage of human-interactive approach includes, but not limited to inaccuracy in the placement of

control points, inconsistency of the fusion results, and the significantly increased interaction time during manual adjustment of the control points. The average time for human manual fusion is about 35 min, including initial control point selection, manual adjustment of control points' coordinates, and evaluation of the fusion result after each adjustment.

Ma proposed a uniform spatial sub-sampling approach, vector quantization algorithm, and stratified sampling with centroid refinements strategy in [24]. Among these three approaches, stratified sampling with centroid refinements strategy achieved shortest average running time of 11 min for a satisfactory fusion result. Matsopoulos and Mouravliansky proposed an automatic retinal image fusion scheme using global optimization techniques in [21]. They reported an average execution time of 4.5 min. Airborne Underwater Geophysical Signals (AUG Signals), Toronto, Canada, has developed an image registration software capable of automatically registering temporal hyperspectral, polarimetric Synthetic Aperture Radar (SAR) or multi-sensor images [25]. AUG Signals' software running time is from 3–7 min. With no more than 1 min running time, the AFEA and HOA algorithms, therefore, has significant advantage compared to other existing image fusion approaches in terms of running time (Table 5).

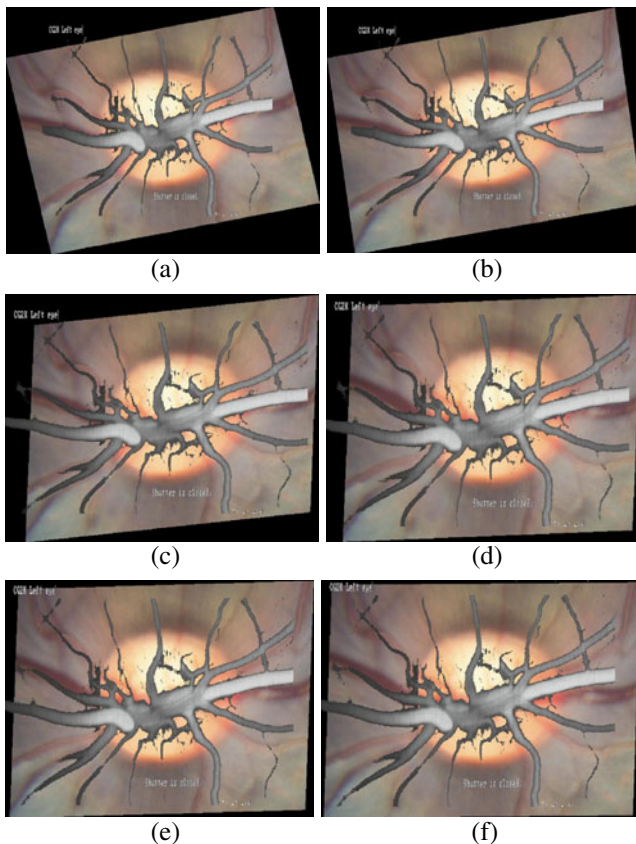


Figure 12 Fused image using RMSE objective function. RMSE (a)–(f)=119.51, 99.54, 71.34, 64.76, 57.01, 49.30.

Table 5 Running time comparison.

Methods	Running time
Manual approach	35 minutes
Uniform spatial sub-sampling	24 minutes
Vector quantization algorithm	19 minutes
Stratified sampling	11 minutes
Matsopoulos's method	4.5 minutes
AUG Signals	3 minutes
AFEA and HOA algorithms	< 1 minute

5 Conclusions

This study has made two new and unique contributions to the multi-modality medical image fusion area in terms of novelty, efficiency, and accuracy. The first contribution is the new automated control point detection AFEA algorithm. The evaluation study with the Centerline Control Point Selection Algorithm shows the advantage of the AFEA. The second contribution is the HOA algorithm for the initial guess of control points' optimization. Building initially on existing work, such as binarization and edge extraction, the proposed approach is in fact a series of algorithms designed to work together to solve the image fusion automation problem. The experiments have also highlighted areas of potential improvement of clinical tools for retinopathy diagnosis. In future research, it would be of interest to expand the AFEA and HOA algorithms for human or animals' 3D eye, brain, or body image fusion for widespread use.

Acknowledgment The authors are grateful to Dr. Thompson and Dr. Ning for their support and help during this research. This work is funded by BCVC programs.

References

- Wong, A., & Orchard, J. (2009). Robust multimodal registration using local phase-coherence representations. *Journal of Signal Processing Systems*, 54(1–3), 89–100.
- Yang, G., Stewart, C., Sofka, M., & Tsai, C. (2007). Registration of challenging image pairs: initialization, estimation, and decision. *IEEE Transactions on Pattern Analysis and Machine Intelligence*, 29(11), 1973–1989.
- Woo, J., Hong, B., Hu, C., Shung, K., Kuo, C., & Slomka, P. (2009). Non-rigid ultrasound image registration based on intensity and local phase information. *Journal of Signal Processing Systems*, 54(1–3), 33–43.
- Loeckx, D., Slagmolen, P., Maes, F., Vandermeulen, D., & Suetens, P. (2010). Nonrigid image registration using conditional mutual information. *IEEE Transactions on Medical Imaging*, 29(1), 19–29.
- Estevez, P., Tesmer, M., Perez, C., & Zurada, J. (2009). Normalized mutual information feature selection. *IEEE Transactions on Neural Networks*, 20(2), 189–201.
- Lin, F., & Olivo, M. (2009). Guest editors' comments; the state-of-the-art technologies for medical and biological imaging. *Journal of Signal Processing Systems*, 54(1–3), 1–6.
- Stewart, C., Tsai, C., & Roysam, B. (2003). The dual-bootstrap iterative closest point algorithm with application to retinal image registration. *IEEE Transactions on Medical Imaging*, 22(11), 1379–1394.
- Canny, J. (1986). A computational approach to edge detection. *IEEE Transactions on Pattern Analysis and Machine Intelligence*, 8, 679–698.
- Chen, X., Yang, J., Zhang, J., & Waibel, A. (2002). Automatic detection of signs with affine transformation. *6th IEEE Workshop on Applications of Computer Vision*, 32–36.
- Khoobehi, B., Beach, J., & Kawano, H. (2004). Hyperspectral imaging for measurement of oxygen saturation in the optic nerve head. *Investigative Ophthalmology & Visual Science*, 45, 1464–1472.
- Beach, J., Ning, J., & Khoobehi, B. (2007). Oxygen saturation in optic nerve head structures by hyperspectral image analysis. *Current Eye Research*, 32, 161–170.
- Otsu, N. (1979). A threshold selection method from gray-level histograms. *IEEE Transactions on Systems, Man, and Cybernetics*, 9, 62–66.
- Sezgin, M., & Sankur, B. (2004). Survey over image thresholding techniques and quantitative performance evaluation. *Journal of Electronic Imaging*, 13, 146–165.
- Chaudhuri, S., Chatterjee, S., & Katz, N. (1989). Detection of blood vessels in retinal images using two-dimensional matched filters. *IEEE Transactions on Medical Imaging*, 8, 263–269.
- Can, A., Shen, H., Turner, J. N., Tanenbaum, H. L., & Roysam, B. (1999). Rapid automated tracing and feature extraction from retinal fundus images using direct exploratory algorithms. *IEEE Transactions on Information Technology in Biomedicine*, 3, 125–138.
- Poli, R., & Valli, G. (1996). An algorithm for real-time vessel enhancement and detection. *Computer Methods and Programs in Biomedicine*, 52, 1–22.
- Antania, S., Leeb, D., Longa, R., & Thoma, G. (2004). Evaluation of shape similarity measurement methods for spine x-ray images. *Journal of Visual Communication and Image Representation*, 15, 285–302.
- Arkin, E. M., Chew, L. P., Huttenlocher, D. P., Kedem, K., & Mitchell, J. (1991). An efficiently computable metric for comparing polygonal shapes. *IEEE Transactions on Pattern Analysis and Machine Intelligence*, 13(3), 209–216.
- Avis, D., & ElGindy, H. (1983). A combinatorial approach to polygon similarity. *IEEE Transactions on Information Theory*, IT-2, 148–150.
- Zhu, Y. (2007). Mutual information-based registration of temporal and stereo retinal images using constrained optimization. *Computer Methods and Programs in Biomedicine*, 86, 210–215.
- Matsopoulos, G., Mouravliansky, N., & Delibasis, K. (1999). Automatic retinal image registration scheme using global optimization techniques. *IEEE Transactions on Information Technology in Biomedicine*, 3, 47–60.
- Doldberg, D. (1989). *“Genetic algorithms in optimization”; search and machine learning*. MA: Addison-Wesley.
- Laliberte, F., & Gagnon, L. (2003). Registration and fusion of retinal images—An evaluation study. *IEEE Transactions on Medical Imaging*, 22(5), 661–673.
- Ma, B. (2001). Parametric and nonparametric approaches for multisensor data fusion. *PhD dissertation; University of Michigan*.
- Airborne Underwater Geophysical Signals (AUG Signals); Automatic image registration—temporal, multi-sensor and multi-layer registration. Toronto, Canada.



Hua Cao received the B.E. degree of Management Information Systems from University of Finance and Economics, China in 2000, the M.S. degree of Systems Science from Louisiana State University, USA in 2003, and the Ph.D. degree of Computer Science from Louisiana State University, USA in 2008. She is a Senior Research Scientist in the Computer Science Department and Ophthalmology Department at Louisiana State University. Dr. Cao has more than 10 research publications including one book, one book chapter, three journals and six conference proceedings. Her research interests include, biomedical imaging, feature detection, data registration, image fusion, artificial intelligence, and route planning.



Bahram Khoobei received the Ph.D. degree in physics from North Texas State University, Denton. He is currently a Professor of Ophthalmology, Louisiana State University Health Sciences Center, Department of Ophthalmology, New Orleans, and also an Adjunct Associate Professor of Biomedical Engineering, at Tulane University School of Engineering, New Orleans. His research interests include hyperspectral imaging to measure oxygen saturation in the retina and optic nerve head; targeting dye and drug delivery systems to the retina; and, retinal blood flow.



Nathan Brener received the B.A. degree of Physics from Brandeis University in 1965 and the Ph.D. degree of Physics from Louisiana State University in 1971. He is a faculty member of Computer Science Department, Louisiana State University. He has approximately 35 years experience in the development of fast algorithms for high performance computing. Dr. Brener has more than 50 research publications in refereed journals and has made numerous presentations at scientific meetings. His research interests include predictive intelligence, artificial intelligence, route planning algorithms, image processing, and parallel processing.



S. Sitharama Iyengar (M'88-SM'89-F'95) received the M.S. degree from the Indian Institute of Science, Bangalore, in 1970 and the Ph.D. degree from Mississippi State University in 1974. He is the chairman and Roy Paul Daniels Chaired Professor of Computer Science at Louisiana State University, Baton Rouge, and is also the Satish Dhawan Chaired Professor at the Indian Institute of Science. His publications include 13 books (Prentice-Hall, CRC Press, IEEE Computer Society Press, John Wiley & Sons, etc.) and more than 280 research papers. He is the founder and editor-in-chief of the International Journal of Distributed Sensor Networks. He has been involved with research in high-performance algorithms, data structures, sensor fusion, data mining, and intelligent systems. Dr. Iyengar was awarded the Distinguished Alumnus Award by the Indian Institute of Science in March 2003. He has served as an associate editor for the IEEE and as a guest editor for the IEEE Transactions on Knowledge and Data Engineering, the IEEE Transactions on Systems, Man, and Cybernetics, and the IEEE Transactions on Software Engineering. He is a fellow of the IEEE, the ACM, and the AAAS.